Photoluminescence of $HgTe/Hg_{1-x}Cd_xTe$ superlattices and a study of minibands

C. R. Becker,[1,*] S. D. Hatch,[2] F. Goschenhofer,[1] V. Latussek,[1] J. M. Dell,[2] and L. Faraone[2]
[1]*Physikalisches Institut der Universität Würzburg, Am Hubland, D-97074 Würzburg, Germany*
[2]*School of Electrical, Electronic and Computer Engineering, The University of Western Australia, Crawley 6009, Australia*
(Received 21 November 2006; revised manuscript received 12 January 2007; published 13 March 2007)

It has been demonstrated that two closely spaced peaks in the infrared absorption spectra of several $HgTe/Hg_{1-x}Cd_xTe$(112)B superlattices (SL's) are due to the $H1$-$E1$ intersubband transition at the center of the Brillouin zone and the zone boundary. The miniband width agrees well with (8×8 $\boldsymbol{k}\cdot\boldsymbol{p}$) calculations. The intersubband transition energies of SL's with both large and small miniband widths have been compared with photoluminescence (PL) spectra over a temperature range of 5–300 K for a number of superlattices with band gaps between 100 and 510 meV at 5 K. The band gap as determined from the peak of the first derivative of the absorption coefficient, i.e., the corresponding intersubband transition energy, agrees well with the PL peak energy. With increasing temperature the PL peak energy increases faster than the band gap by a range of factors given by $0.25-0.75k_BT$, however, which are well within the width of the thermally broadened PL peaks.

DOI: 10.1103/PhysRevB.75.115115 PACS number(s): 78.20.Bh, 78.20.Ci, 78.30.Fs

I. INTRODUCTION

The optical properties of the $HgTe/Hg_{1-x}Cd_xTe$ superlattice (SL) are of fundamental interest as well as potentially useful for infrared optoelectronic applications,[1–3] particularly in the far-infrared region.

The quantum confined states in infinitely separated multiple quantum wells (MQW's) develop into minibands if the separation between the QW's is reduced. The corresponding miniband width increases with decreasing separation with the transition from MQW to SL. Minibands have been investigated primarily in GaAs based superlattices[4] and to a lesser extent in CdTe/CdMnTe superlattices[5] by the modulation techniques of piezomodulated reflectivity and photoreflectance as well as photoluminescence (PL) and photoluminescence excitation (PLE). PL spectra must be supplemented by other methods because they reveal only the lowest intersubband transition. However, this is not the case for PLE. Using these methods the above mentioned investigations probe excitons associated with subband dispersion in these wide band gap superlattices. To our knowledge minibands have not previously been directly investigated in HgTe based narrow gap superlattices by optical methods.

The PL double peaks observed by Meyer *et al.*[6] in $HgTe/Hg_{1-x}Cd_xTe$ SL's were shown to be due to monolayer fluctuations in the layers. In this investigation, the results of optical absorption experiments on $HgTe/Hg_{1-x}Cd_xTe$ superlattice are compared with those of PL for temperatures between 5 and 300 K. Experimental evidence of minibands, i.e., two closely spaced peaks or a peak with a pronounced shoulder, have been observed in absorption spectra and compared to theoretical calculations.

In order to compare photoluminescence results with absorption spectra and ultimately with the intersubband transition itself, one has to determine the relevant experimental intersubband transition energies. This can be done by taking the absorption edge which is defined by the peak position of the first derivative of the absorption coefficient (α) and is in very good agreement with the intersubband energy itself as has been previously demonstrated.[7]

II. EXPERIMENTAL AND THEORETICAL DETAILS

Epitaxial growth was carried out either in a Riber 2300 molecular beam epitaxial (MBE) system[7] or a Riber 32 MBE.[8] After the growth of a thin CdTe buffer layer, the $HgTe/Hg_{1-x}Cd_xTe$ superlattices were grown on (112)B or (001) oriented $Cd_{0.96}Zn_{0.04}Te$ substrates at 180 °C. The substrate temperature was determined with an accuracy of ±2 °C by means of a thermocouple which was in physical contact with a molybdenum substrate holder. The thermocouple was carefully calibrated at the melting points of indium and tin.

The composition of the barrier material[9] has been determined by means of transmission measurements on several thick test layers of $Hg_{1-x}Cd_xTe$ grown under similar conditions. At a growth temperature of 180 °C, $x=0.95\pm0.02$ and $x=0.70\pm0.02$ for the (112)B and (001) orientations, respectively. This was found to be the case regardless of the thermal history of the MBE chamber prior to growth. Furthermore, from the measured phonon frequencies, the $Hg_{1-x}Cd_xTe$ alloy composition of the barriers in (001) oriented SL's was shown to agree with the above value.[10]

The superlattice period has been determined by x-ray diffraction, and the well and barrier thicknesses have been determined from a simulation of the x-ray diffraction and the optical absorption, i.e., the dependence of intersubband transitions on well and barrier thicknesses.[7]

Optical transmission measurements were carried out with a Fourier transform spectrometer, Bruker IFS88. A deuterated triglycine sulfate detector was usually employed rather than a liquid-nitrogen-cooled detector, e.g., $Hg_{1-x}Cd_xTe$, because of its better linearity. The aperture was kept as small as possible for the same reason, i.e., a diameter of 2–3 mm. A dewar with ZnSe windows was employed for the low-temperature measurements, which limited the transmission to energies above approximately 60 meV or wavelengths below 20 μm. The absorption coefficient was determined by fitting the experimental transmission spectra to a theoretical description of the multilayer system using standard matrix procedures.[11]

PL measurements were conducted either with a Fourier transform spectrometer, Bruker IFS88, or a SPEX 750M monochromator using either a liquid-nitrogen-cooled $Hg_{1-x}Cd_xTe$ or InSb detector. The PL was activated by a GaAs based laser diode in the former device and an argon ion laser in the latter. The intensity of the focused beams was on the order of $1-2$ W/cm^2. A double modulation technique was employed in the Fourier transform spectrometer in order to eliminate black-body radiation.

A large number of band-structure calculations for the $HgTe/Hg_{1-x}Cd_xTe$ superlattice have been published during the last decade.[12–15] Ram-Mohan *et al.*[13] employed the envelope function method and developed a transfer-matrix procedure to calculate the superlattice states. They accounted for the full 8×8 Kane Hamiltonian including all second-order terms representing the far-band contributions, but did not apply their results to a calculation of the optical constants. On the other hand, Johnson *et al.*[14] applied a slightly different version of the envelope function method, and deduced optical constants from their superlattice energies and eigenfunctions. But in their approach they used a simplified band model, which omits all the second-order far-band contributions, with the exception of a finite heavy hole mass. In order to overcome these shortcomings, we have combined the essential aspects of both approaches.[16] This enables us to calculate the optical constants based on a realistic band-structure model, which includes all second-order higher band contributions.

A revised set of values for the band parameters deduced from measurements on bulk HgTe and $Hg_{1-x}Cd_xTe$ by Weiler[17] were employed which, nevertheless, reproduce the same bulk band structure ($\Delta=1.0$ eV, $\gamma_1=4.1$, $\gamma_2=0.5$, $\gamma_3=1.3$, $F=0$, and $E_p=18.8$ eV). The effective heavy-hole mass was taken to be linearly temperature dependent,[7] i.e., $m^*_{hh}=0.53$ and $0.79m_0$ at 5 and 300 K, respectively, for the (112)B orientation, and $m^*_{hh}=0.32$ and $0.40m_0$ at 5 and 300 K, respectively, for the (001) orientation.[7]

The SL band structure is primarily determined by that of the well and is influenced to a much lesser degree by the band structure of the barrier. Therefore the above values were employed for both the HgTe wells and the $Hg_{1-x}Cd_xTe$ barriers. According to Weiler[17] the only parameter that changes significantly with alloy composition and temperature is the energy gap.

The valence-band offset between HgTe and CdTe,

$$\Lambda(T) = \Lambda_0 + \frac{d\Lambda}{dT}T, \tag{1}$$

according to Becker *et al.*[7] was employed, where $\Lambda_0=570$ meV and $d\Lambda/dT=-0.40$ meV/K. Furthermore, $\Lambda(T)$ was assumed to vary linearly with x for $Hg_{1-x}Cd_xTe$.[18] An interface width which results during growth or from interdiffusion of the two types of layers was integrated into the theory. The concentration profile across the interface is described by an error function similar to an experimental profile according to Kim *et al.*[19]

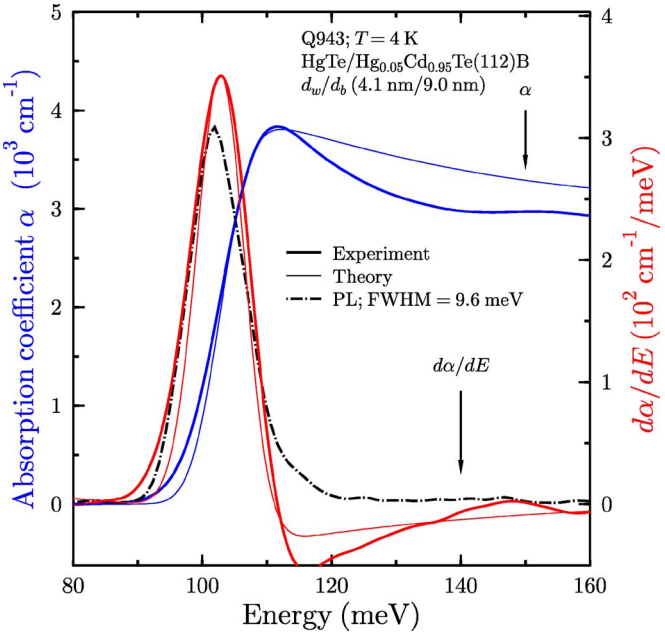

FIG. 1. (Color online) The experimental and theoretical (thick and thin lines) absorption coefficients and their first derivatives as well as the photoluminescence (dashed-dotted line) of the $HgTe/Hg_{1-x}Cd_xTe$(112)B SL Q943 at 4 K.

III. RESULTS AND DISCUSSION

A. Optical band gap and photoluminescence

The experimental and theoretical absorption coefficients together with their first derivatives ($d\alpha/dE$) for the SL Q943 at 4 K are displayed in Fig. 1. Good agreement for both is obvious as well as the good agreement between the peak energies of $d\alpha/dE$ for the $H1-E1$ intersubband transition and the PL spectrum, where H and E refer to heavy hole and electron subbands. In order to reproduce the width of the absorption edge, i.e., the linewidth of $d\alpha/dE$, a Gaussian distribution of the HgTe and $Hg_{1-x}Cd_xTe$ layer thicknesses with a standard deviation of 0.45 monolayers (MLs) was employed in this calculation.

It can be easily shown that the division of two transmission spectra at two adjacent temperatures is related to the change in the absorption coefficient, i.e., $T_{T+\Delta T}/T_{T-\Delta T}-1 \approx \Delta\alpha$. The use of this method can reduce experimental uncertainties inherent in the calculation of α and those due to the presence of interference fringes. Good agreement between experiment and theory for $T_{T+\Delta T}/T_{T-\Delta T}-1$ and $d\alpha/dE$ is demonstrated in Fig. 2. Due to the wide barriers the miniband width of 0.5 meV is extremely narrow as indicated by the vertical band in Fig. 2.

The peak energy of the the PL spectrum at 20 K also agrees with the absorption edge, although it is about 2 meV lower due to a small Burstein-Moss shift[20] of the absorption edge. Of particular significance is the good agreement between the lower energy flank of the PL and the absorption edge defined by $d\alpha/dE$, as well as their widths. This indicates that the PL is due solely to band-to-band transitions with nearly the same transition probabilities as that of optical absorption.

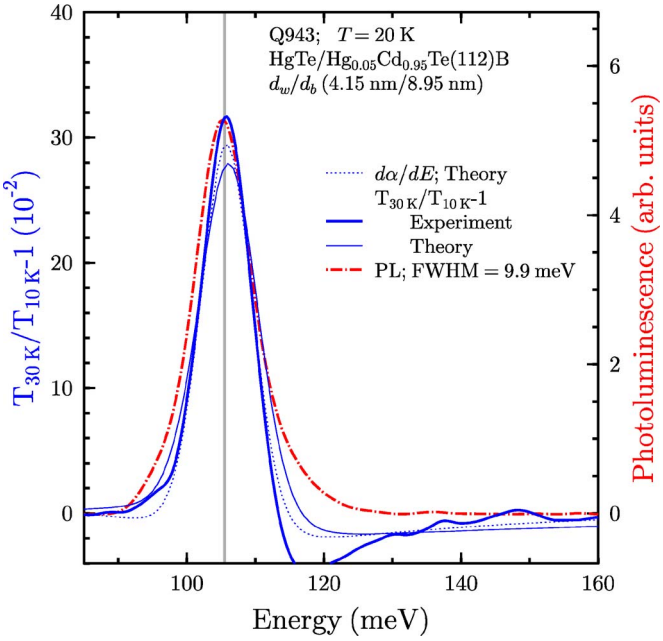

FIG. 2. (Color online) The division of experimental (thick line) and theoretical (thin line) transmission spectra at neighboring temperatures ($T_{30\,K}/T_{10\,K}-1$), the theoretical $d\alpha/dE$ (dotted line) spectrum, and the PL spectrum (dashed-dotted line) for the SL Q943 at 20 K. The miniband width is indicated by the gray vertical band.

The $d\alpha/dE$ and PL spectra for the (001) oriented SL Q424 shown in Fig. 3 are asymmetric and, as expected, the presence of an Urbach tail[21] on the lower energy flank cannot be satisfactorily reproduced by $(8\times 8\boldsymbol{k}\cdot\boldsymbol{p})$ theory. The PL peak lies significantly below that of $d\alpha/dE$ and the onset of

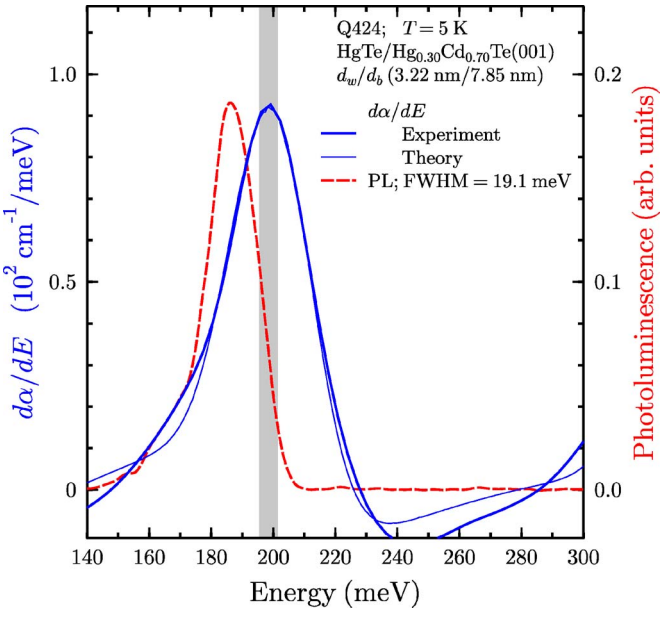

FIG. 3. (Color online) The experimental (thick line) and theoretical (thin line) $d\alpha/dE$ spectra, and the PL spectrum (dashed line) for the SL Q424 at 5 K. The miniband width is indicated by the gray vertical band.

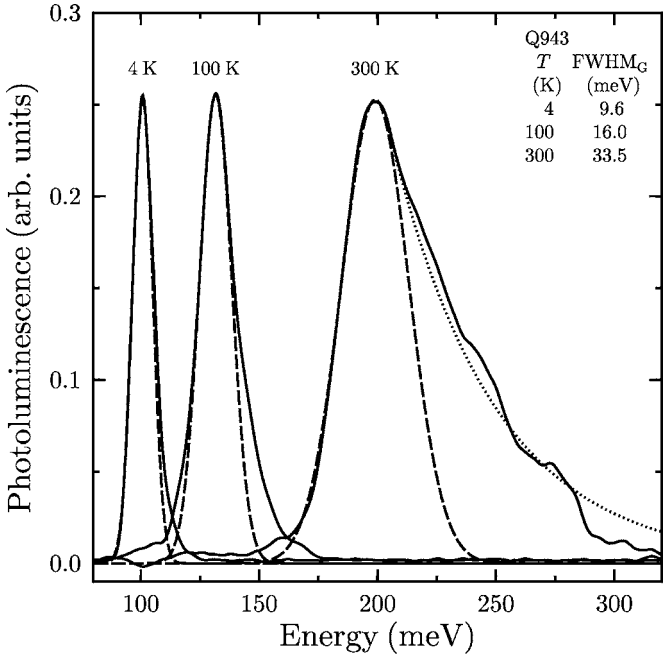

FIG. 4. PL spectra at 4, 100, and 300 K (solid lines) together with Gaussian simulations of the data (dashed lines) and an exponential fit of the high-energy flank of the 300 K PL spectrum (dotted line) for the SL Q943. The peak amplitudes are normalized to the value at 4 K.

PL occurs near the pronounced low-energy tail. This is in contrast to the (112)B oriented SL's, whose $d\alpha/dE$ peak either coincides with the PL peak for the low-energy gap SL's, or occurs less than 7 meV above the PL peak for the three SL's with higher band gaps. Furthermore, a standard deviation of 1.02 MLs for the HgTe and $Hg_{1-x}Cd_xTe$ layer thicknesses was necessary in the Gaussian distribution in order to reproduce the width of the absorption edge. This value is approximately two to three times larger than that of the (112)B oriented SL's, which can be explained by a larger alloy fluctuation in the (100) barriers due to their x value of 0.70 ± 0.02 as opposed to 0.95 ± 0.02. The absence of a low-energy tail or a significantly smaller low-energy tail in the (112)B SL's is also a consequence of the expected smaller alloy fluctuations in the nearly binary barriers.

A homogeneous charge-carrier distribution within a random potential yields an exciton line shape of Gaussian form,[22]

$$f(E) = 1/(\sqrt{2\pi}\sigma_p)\exp\left[-\frac{1}{2}\left(\frac{E-E_p}{\sigma_p}\right)^2\right]. \qquad (2)$$

Even though the excitonic binding energy is negligible and no evidence for an exciton exists in this system, electrons and holes are generated and a Gaussian distribution describes the low-temperature PL spectra of the (112)B SL's with low band-gap energies very well, see Fig. 4, and that of the three (112)B SL's with larger band-gap energies reasonably well. Moreover, $d\alpha/dE$ for the (112)B SL's with a single peak have been fit with a Gaussian distribution with good agreement. This is also the case for the SL's with two peaks or a

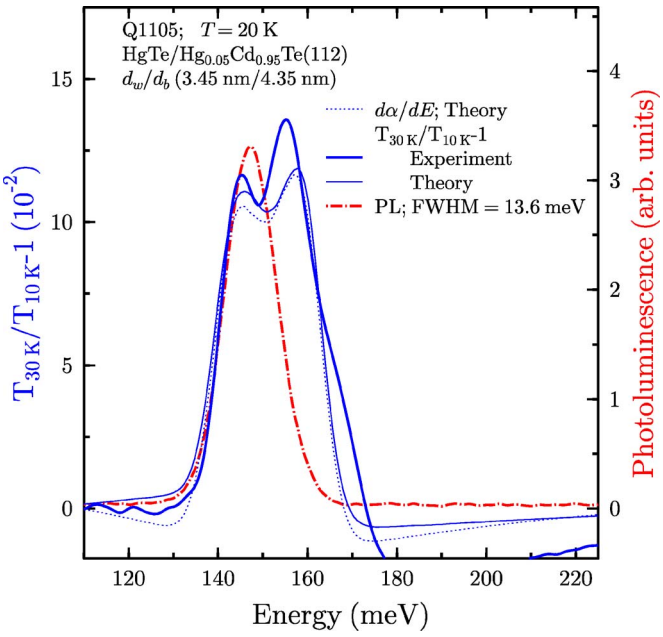

FIG. 5. (Color online) The experimental (thick line) and theoretical (thin line) $T_{30\,K}/T_{10\,K}-1$ spectra, the theoretical $d\alpha/dE$ (dotted line) spectrum, and the PL spectrum (dashed-dotted line) for the SL Q1105 at 20 K.

peak with a shoulder with the exception of the high-energy flank, see, for example, Fig. 5. HgTe and $Hg_{1-x}Cd_xTe$ thicknesses, $H1$-$E1$ intersubband transition energies, and the full width at half maximum assuming a Gaussian distribution ($FWHM_G = 2.355\sigma_p$) of the peaks in $d\alpha/dE$ and PL at 5 K are listed in Table I for all investigated SL's.

As can be seen from the results in Table I, $FWHM_G$ of the peaks in $d\alpha/dE$ and PL increases roughly with increasing $H1$-$E1$ transition energy, with several exceptions because the overlap of the $H1$-$E1$ components at the center ($\boldsymbol{q}=0$) and edge ($\boldsymbol{q}=1$) of the Brillouin zone shown in Fig. 6, depend on several factors, i.e., on the linewidth of $d\alpha/dE$ and the separation of the $\boldsymbol{q}=0$ and $\boldsymbol{q}=1$ components together with the position of the Fermi energy. Nevertheless, simulations of $d\alpha/dE$ for all SL's using a Gaussian distribution of the HgTe and $Hg_{1-x}Cd_xTe$ layer thicknesses with a standard deviation of 0.30–0.45 ML are in good agreement with experiment for all (112)B oriented SL's as shown, for example, in Figs. 2, 5, and 7. The relative magnitude of the necessary Gaussian distribution for these simulations increases with decreasing well thickness and is consequently responsible for the increase in width of the structure in $d\alpha/dE$ and consequently that of PL. This is evidence of the excellent homogeneity of the HgTe and $Hg_{1-x}Cd_xTe$ layer thicknesses in these (112)B SL's.

B. Miniband width

If the $Hg_{1-x}Cd_xTe$ barrier thickness is reduced, such that the miniband width is significantly larger than that of the absorption edge and, in addition, the Fermi energy is near or below the $E1$ subband energy at $\boldsymbol{q}=0$, then two peaks should be observed. Indeed this is the case for Q1105 and Q2177 as shown in Fig. 5 for Q1105. In addition, a peak with an unresolved shoulder is observed in the absorption spectra of Q1106 and SDH25 as shown in Fig. 7 for Q1106.

The theoretical separation of the $H1$-$E1$ intersubband transitions at the center and edge of the Brillouin zone for Q1105 at 20 K is 20.5 meV, whereas the experimental and theoretical values for $d\alpha/dE$ are 10.0 and 11.8 meV, respec-

TABLE I. The HgTe and $Hg_{1-x}Cd_xTe$ layer thicknesses (d_w and d_b); $H1$-$E1$ intersubband transition energies at 5 and 80 K; the FWHM assuming a Gaussian distribution ($FWHM_G$) for the PL and $d\alpha/dE$ peaks at 5 K; the miniband width (δ) of the $H1$-$E1$ intersubband transition at 5 K resulting from the calculated intersubband transition energies at $\boldsymbol{q}=0$ and $\boldsymbol{q}=1$, and from the separation of the two peaks in the theoretical and experimental absorption coefficients; and the difference in temperature dependence ν from Eq. (4) for all investigated SL's.

			$E_{H1\text{-}E1}$		$FWHM_G$ (5 K)		δ (5 K)			
								$E_{p2}-E_{p1}$		
SL	d_w nm	d_b nm	5 K meV	80 K meV	PL meV	$d\alpha/dE$ meV	$E_{q=1}-E_{q=0}$ theory meV	theory meV	expt. meV	ν
(112)B										
Q943	4.15	8.95	103	125	9.6	8.2	0.5			0.25
Q1104	3.90	4.50	108	130	9.5	13.0	17.5			0.28
Q1105	3.45	4.35	140	163	13.0	10.0	20.5	11.8	10.0	0.43
Q1103	3.20	4.50	177	198		21.2	18.5			0.60
Q1106	2.93	3.77	239	259	16.7	16.5	32.0	18[a]	18[a]	0.47
Q2177	2.36	3.74	310	327	19.1	18.3	39.8	28.6	30.3	0.65
SDH25	2.29	4.10	343	359	14.2	15.3	28.7	18[a]	16[a]	0.75
SDH24	1.60	4.05	510	524	21.2	33.0	36.0			0.62
(001)										
Q424	3.22	7.85	198	221	19.1	32.7	6.0			0.89

[a]Results from a Gaussian fit of the corresponding peak and shoulder.

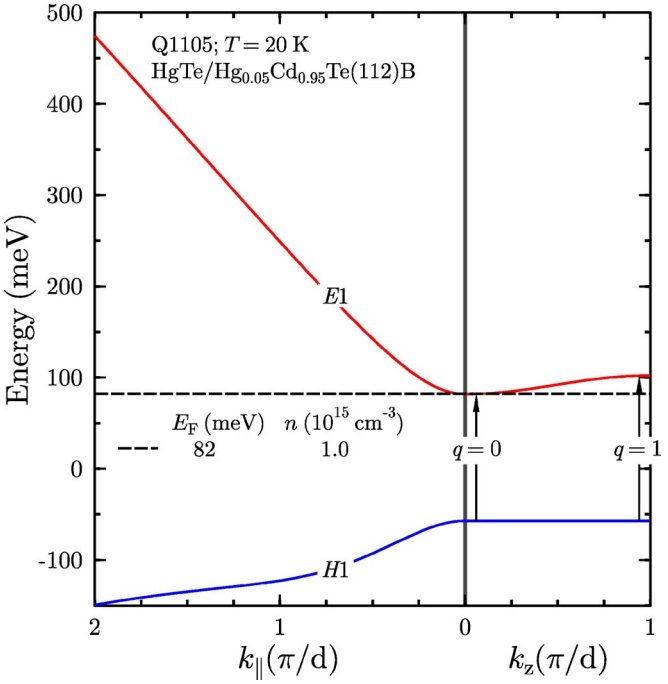

FIG. 6. (Color online) The band structure (solid lines) of the SL Q1105 at 20 K in the SL plane ($\boldsymbol{k}_\parallel$) and perpendicular to the plane ($\boldsymbol{k}_z$), where d is the SL period. The center ($\boldsymbol{q}=0$) and edge ($\boldsymbol{q}=1$) of the Brillouin zone are indicated by vertical arrows and the Fermi energy for a carrier concentration of 1.0×10^{15} cm^{-3} is shown as a dashed line.

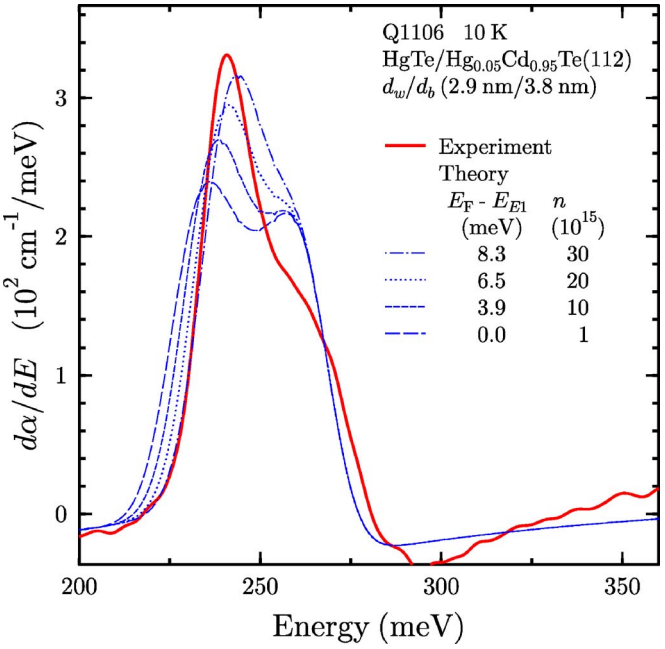

FIG. 7. (Color online) The experimental (thick line) and theoretical (thin lines) $d\alpha/dE$ spectra for different charge carrier concentrations and consequently different Fermi energies (E_F) for the SL Q1106 at 10 K.

tively. The discrepancy in energy separation between the $H1$-$E1$ intersubband transitions and the two $d\alpha/dE$ peaks is caused by the close proximity of the two transitions as well as by transitions at positions in the Brillouin zone between the center and edge where the density of states is lower but significant. Indeed, agreement is good between the experimental and theoretical values of the separation in $d\alpha/dE$ mentioned above, as well as the corresponding values in $T_{30\ K}/T_{10\ K}-1$, i.e., 11.0 and 11.8 meV, respectively. Moreover, agreement between experiment and theory is good for the two SL's with two resolved peaks and the two SL's with a peak and shoulder, see Table I.

Another explanation of the presence of two closely spaced absorption peaks could be as follows: If two SL's with the necessary HgTe thicknesses were present then two absorption peaks would be observed. However, two peaks in the x-ray-diffraction spectra corresponding to each satellite should also be observed and this is not the case. For example the two peaks for each of the +1 and −1 satellites in the x-ray-diffraction spectrum of Q1106 would need to be separated by 100 arcsec, however, only one peak with a full width at half maximum (FWHM) of 60 and 64 arcsec, respectively, are visible. Hence we can definitely rule out this possibility.

The lower energy edge of the PL spectrum coincides very well with the lower energy edge of $d\alpha/dE$ as can be seen in Fig. 5. This is also true for the energy of the peak in the PL spectrum and the lower energy peak in the absorption spectrum.

The relative intensities of the two peaks corresponding to the center and edge of the Brillouin zone are strongly dependent on the charge-carrier concentration and hence the Fermi energy. This is demonstrated by the results for Q1106 in Fig. 7; the intensities of the two peaks in $d\alpha/dE$ are roughly equivalent when $n=1.0\times10^{15}$ cm^{-3}, whereas $n=2-3\times10^{16}$ cm^{-3} is necessary in order to reproduce the experimental peak with a shoulder on the high-energy side. This is consistent with the large free carrier absorption observed in this SL.

Only a weak shoulder was observed on the peak in $d\alpha/dE$ for Q1104 and none on the peak in Q1103 and SDH24. This is due to the fact that their miniband width is comparable to their FWHM in combination with the presence of the Fermi energy near the center of the miniband for Q1103 and Q1104.

C. Temperature dependence

The PL spectra at lower temperatures can be simulated by a Gaussian distribution as can be seen in Fig. 4. Even at higher temperatures a reasonably good simulation of the low-energy flank as well as the peak is possible as shown also in Fig. 4. As demonstrated in Fig. 4, the high energy flank at higher temperatures can be reproduced by an exponential function;

$$I = I_\circ \exp[-(E-E_p)/(ck_BT)], \tag{3}$$

where E_p is the peak energy plus a small shift to the high-energy flank of about 2–4 meV and $c=1.7$ for Q943. c lies between 1.4 and 1.7 for all investigated (112)B SL's.

The FWHM$_G$ values for Q943 of the PL and $d\alpha/dE$ peaks as well as their differences for temperatures between 4 and 300 K are plotted in Fig. 8. As can be seen in Table I, the

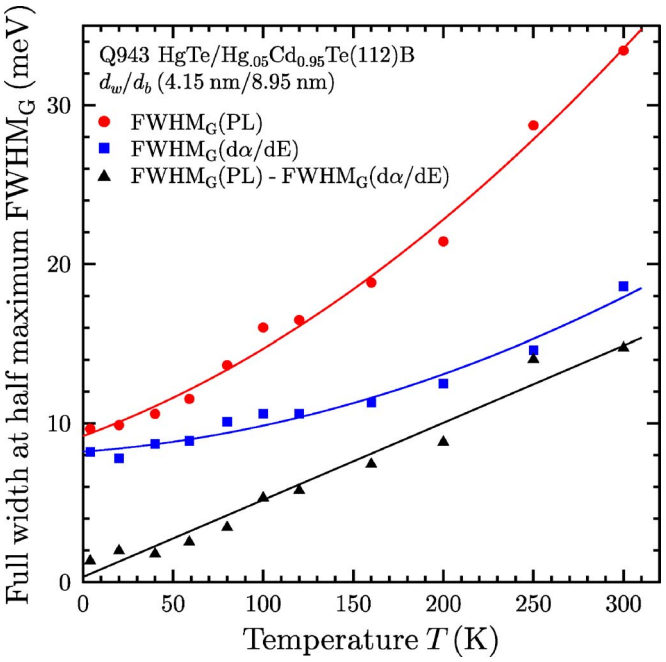

FIG. 8. (Color online) The $FWHM_G$ values for Q943 of the PL and $d\alpha/dE$ peaks as well as their differences for temperatures between 4 and 300 K. The lines are quadratic and linear fits of the experimental data.

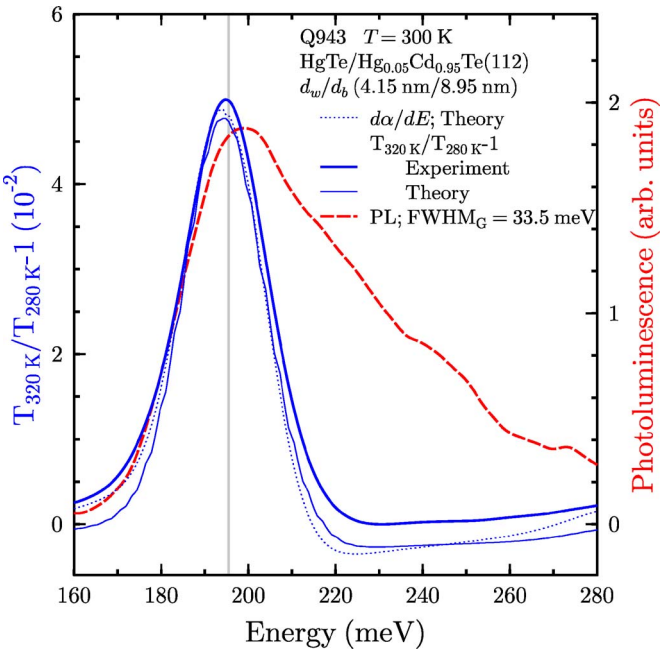

FIG. 9. (Color online) The experimental (thick line) and theoretical (thin line) $T_{320\ K}/T_{280\ K}-1$ spectra, the theoretical $d\alpha/dE$ (dotted line) spectrum, and the PL spectrum (dashed line) for the SL Q943 at 300 K.

$FWHM_G$ of the PL peak is about the same size or slightly larger than that of the $d\alpha/dE$ peak at low temperatures. This is true for most of the SL's with the exceptions of Q1104, Q1103, and SDH24 which have an unresolved $d\alpha/dE$ peak. In the case of Q1104 and Q1103 this is caused by an appreciable shift of the Fermi energy toward the center of the miniband and in the case of SDH24 it is due to the relatively broad absorption edge.

The $FWHM_G$ of the PL peak increases faster with increasing temperature than that of $d\alpha/dE$. This difference is approximately linear and at 300 K is 15 meV ($0.6k_BT$) for Q943. This is comparable with the thermal broadening factor of $0.7k_BT$ employed in the simulation of $d\alpha/dE$ which is shown in Fig. 9. Similar behavior has been observed and simulated with good agreement for all investigated SL's; The temperature dependence of $FWHM_G$, i.e., $\Delta FWHM_G = FWHM_G(300\ K) - FWHM_G(0\ K)$, lies between 0.94 and $1.24k_B$ for the PL peak and 0.40 and $0.60k_B$ for the $d\alpha/dE$ peak.

The absorption edge of the $H1$-$E1$ transition in Q943 at 300 K as defined by either $d\alpha/dE$ or $T_{320\ K}/T_{280\ K}-1$, coincides very well with the low-energy edge of the PL spectrum, even though the peak of the latter is shifted 6 meV above that of the absorption edge, see Fig. 9. In other words, the onset of absorption and PL occur at nearly the same energy.

The peak energies for the PL as well as for the $T_{T+20\ K}/T_{T-20\ K}-1$ and $d\alpha/dE$ spectra are plotted as a function of temperature in Fig. 10. The experimental absorption data (symbols) compare well with theoretically calculated values. The temperature coefficient of the PL data from a least-square fit is larger than that of the absorption data:

$$\frac{dE_{PL}}{dT} - \frac{dE_{H1-E1}}{dT} = \nu k_B, \tag{4}$$

where $\nu=0.25$ for Q943. The values of ν for all of the investigated SL's are listed in Table I.

In order to accurately determine the temperature dependence of the intersubband transitions, precise knowledge of their energies is required. As can be seen in Figs. 2 and 9, the intersubband transition energy and the peak positions of $d\alpha/dE$ and $T_{T+\Delta T}/T_{T-\Delta T}-1$ agree to within 1–2 and 6 meV for Q943 at 5 and 300 K, respectively.

Similar behavior is observed for all temperatures and all investigated (112)B SL's, even though the experimental uncertainties are larger in the SL's whose minibands are wider. These uncertainties of at most 5 meV are due to a lack of knowledge of the Fermi energy at higher temperatures. At low temperatures, the PL peak corresponds to the $H1$-$E1$ transition at the center of the Brillouin zone for the SL's with a resolved wide miniband structure. In SL's with an unresolved miniband whose width is comparable to the $FWHM_G$ of the PL and $d\alpha/dE$, the PL and $d\alpha/dE$ peaks occur near an average of the $H1$-$E1$ transition at the center and edge of the Brillouin zone. At higher temperatures when the thermal energy is comparable to the miniband width, the absorption edge is shifted to the center of the miniband. The values of ν in Table I are based on a shift of the single $d\alpha/dE$ peak for the SL's with unresolved minibands or for SL's with a resolved miniband structure, a shift of the experimental $d\alpha/dE$ peak at $q=0$ to the corresponding calculated $d\alpha/dE$ peak at $q=0$, see Fig. 11. In the latter case, more realistic values of ν based on a shift of the experimental $d\alpha/dE$ peak at $q=0$ to the experimentally determined center of the miniband range

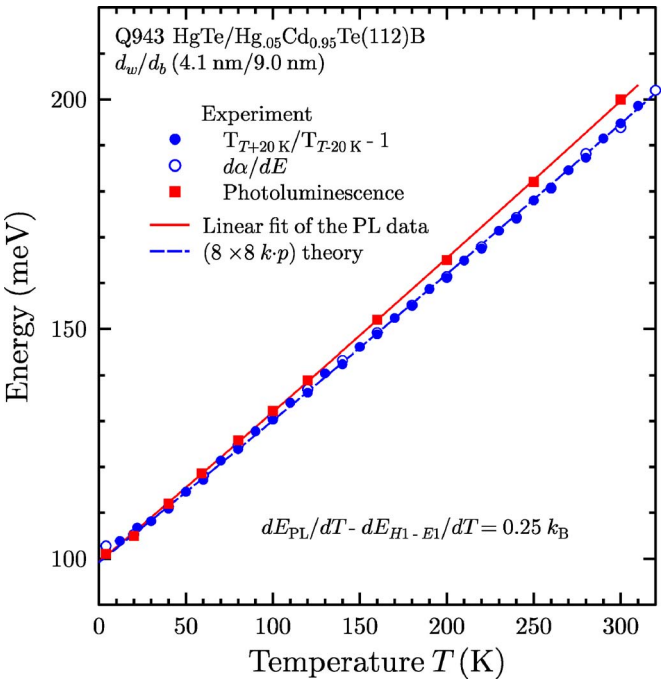

FIG. 10. (Color online) Experimental values of the $H1$-$E1$ intersubband transition energy from $T_{T+20\,K}/T_{T-20\,K}-1$ and $d\alpha/dE$ spectra (circles) and PL peak values (squares) for Q943 as a function of temperature. The solid line represents theoretical absorption results and the dashed line is a least-square linear fit of the PL results.

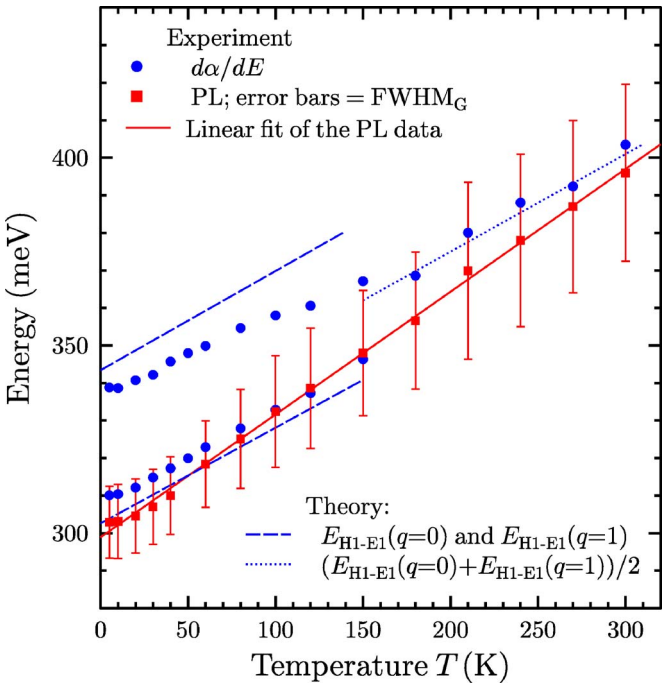

FIG. 11. (Color online) Experimental values of the $H1$-$E1$ intersubband transition energy from $d\alpha/dE$ spectra (circles) and PL peak values (squares) for Q2177 as a function of temperature. The error bars for the PL data are the corresponding FWHM$_G$ values. The dashed lines represent the theoretical $H1$-$E1$ intersubband transition energies at the center and edge of the Brillouin zone and the dotted line represents an average of these two values. The solid line is a least-square linear fit of the PL results and merely a guide to the eye.

from 0.0 to 0.4 for all (112)B oriented SL's as demonstrated in Fig. 11 for Q2177.

Previously, larger values of ν for HgTe/Hg$_{1-x}$Cd$_x$Te SL's have been published; Meyer *et al.*[23] reported a value of $\nu=1.5$ and the results of other investigations[24,25] are consistent with $\nu\approx 1.0$. In these studies the experimental temperature dependences of PL were compared with theoretically calculated temperature dependences of the energy gap. However, more recently it has been shown that in order to correctly reproduce the temperature dependence of the energy gap three criteria must be fulfilled;[7] the first and most important is that the valence-band offset is temperature dependent, see Eq. (1), the second is that the energy gap of HgTe at 300 K must be taken to be −160 meV instead of the previously accepted empirical values of −120 meV (Ref. 9) or −140 meV,[26] and the third is that a linearly temperature-dependent effective heavy-hole mass as mentioned above must be employed. In addition, the large miniband width of most of the previously investigated SL's (Refs. 23 and 24) and uncertainty about the Fermi energy could result in large experimental uncertainties and the larger reported values of ν.

Values of $\nu k_B T$ at room temperature are less than 35% of the FWHM$_G$ of the PL peak for all the SL's in this investigation with the exception of 45% for SDH25. Furthermore, the low-energy flank of the PL peak closely approximates the absorption edge, for example see Figs. 2 and 9. This is true for all SL's with the exception of the SL's with an appreciable Urbach tail or with partially resolved miniband structure. The former statement is valid for the (001) oriented SL and the latter for the two (112)B oriented SL's with larger energy gaps. Hence it is fair to say that these small differences in temperature dependence between PL and the absorption edge, i.e., $d\alpha/dE$, described above, can be explained by thermal broadening effects. Therefore it follows that the PL is due solely to band-to-band transitions with nearly the same transition probabilities as that of optical absorption for all temperatures between 5 and 300 K.

IV. CONCLUSIONS

Two closely spaced peaks or a peak with a pronounced shoulder in the infrared absorption spectra of HgTe/Hg$_{1-x}$Cd$_x$Te(112)B superlattices (SL's) have been observed. They have been shown to be due to the $H1$-$E1$ intersubband transition at the center of the Brillouin zone and the zone boundary. The observed miniband width in the absorption spectra agrees well with that of $(8\times 8\boldsymbol{k}\cdot\boldsymbol{p})$ calculations. The band gap or the intersubband absorption edge defined by $d\alpha/dE$ of SL's with both large and small miniband widths have been compared with PL spectra over a temperature range of 5–300 K for a number of superlattices with band gaps between 100 and 510 meV at 5 K. The band gap, i.e.,

the corresponding intersubband transition energy, agrees well with the PL peak energy. The temperature coefficient of the PL peak energy is larger than that of the band gap by a range of values given by $0.25-0.75k_BT$, albeit more realistic values range from 0.0 to $0.4k_BT$. Moreover, all of these values are much smaller than the width of the thermally broadened PL peaks. Of particular importance is the fact that the onset of PL and absorption coincide within experimental error for the (112)B oriented SL's. In a (001) SL the onset is associated with an Urbach tail on the low-energy flank. We therefore conclude that the PL in the (112)B SL's is due solely to band-to-band transitions with nearly the same transition probabilities as that of optical absorption for all temperatures between 5 and 300 K.

ACKNOWLEDGMENTS

The support of the Deutsche Forschungsgemeinschaft via SFB 410, II-VI Halbleiter: Wachstumsmechanismen, niederdimensionale Strukturen und Grenzflächen, as well as the support of the Australian Research Council and the Australian Research Network for Advanced Materials are gratefully acknowledged.

*Electronic address: becker@physik.uni-wuerzburg.de

[1] J. N. Schulman and T. C. McGill, Appl. Phys. Lett. **34**, 663 (1979).
[2] Y. D. Zhou, C. R. Becker, Y. Selamet, Y. Chang, R. Ashokan, R. T. Boreiko, T. Aoki, D. J. Smith, A. L. Betz, and S. Sivananthan, J. Electron. Mater. **32**, 608 (2003).
[3] Y. Selamet, Y. D. Zhou, J. Zhao, Y. Chang, C. R. Becker, R. Ashokan, C. H. Grein, and S. Sivananthan, J. Electron. Mater. **33**, 503 (2004).
[4] C. Parks, A. K. Ramdas, M. R. Melloch, and L. R. Ram-Mohan, Phys. Rev. B **48**, 5413 (1993), and reference therein.
[5] D. Labrie and J. J. Dubowski, Superlattices Microstruct. **16**, 25 (1994).
[6] J. R. Meyer, A. R. Reisinger, K. A. Harris, R. W. Yanka, and L. M. Mohnkern, Appl. Phys. Lett. **64**, 545 (1994).
[7] C. R. Becker, V. Latussek, A. Pfeuffer-Jeschke, G. Landwehr, and L. W. Molenkamp, Phys. Rev. B **62**, 10353 (2000).
[8] S. D. Hatch, R. H. Sewell, J. M. Dell, L. Faraone, C. R. Becker, and B. Usher, J. Electron. Mater. **35**, 1481 (2006).
[9] J. P. Laurenti, J. Camassel, A. Bouhemadou, B. Toulouse, R. Legros, and A. Lusson, J. Appl. Phys. **67**, 6454 (1990).
[10] M. von Truchseß, V. Latussek, F. Goschenhofer, C. R. Becker, G. Landwehr, E. Batke, R. Sizmann, and P. Helgesen, Phys. Rev. B **51**, 17618 (1995).
[11] D. Fasold, K. Heil, and S. Jetschke, Phys. Status Solidi A **86**, 125 (1984).
[12] J. R. Meyer, C. A. Hoffman, and F. J. Bartoli, Semicond. Sci. Technol. **5**, S90 (1990).
[13] L. R. Ram-Mohan, K. H. Yoo, and R. L. Aggarwal, Phys. Rev. B **38**, 6151 (1988).
[14] N. F. Johnson, H. Ehrenreich, P. M. Hui, and P. M. Young, Phys. Rev. B **41**, 3655 (1990).
[15] A. Simon, D. Bertho, D. Boiron, and C. Jouanin, Phys. Rev. B **42**, 5221 (1990).
[16] E. Bangert, P. Boege, V. Latussek, and G. Landwehr, Semicond. Sci. Technol. **8**, S99 (1993).
[17] M. H. Weiler, *Semiconductors and Semimetals*, edited by R. Willardson and A. C. Beer (Academic Press, New York, 1981), Vol. 16, p. 119.
[18] C. K. Shih and W. E. Spicer, Phys. Rev. Lett. **58**, 2594 (1987).
[19] Y. Kim, A. Ourmazd, M. Bode, and R. D. Feldman, Phys. Rev. Lett. **63**, 636 (1989).
[20] E. Burstein, Phys. Rev. **93**, 632 (1954); T. S. Moss, Proc. Phys. Soc. London, Sect. B **76**, 775 (1954).
[21] F. Urbach, Phys. Rev. **92**, 1324 (1953).
[22] E. F. Schubert and W. T. Tsang, Phys. Rev. B **34**, 2991 (1986).
[23] J. R. Meyer, A. R. Reisinger, K. A. Harris, R. W. Yanka, L. M. Mohnkern, and L. R. Ram-Mohan, J. Cryst. Growth **138**, 981 (1994).
[24] J. P. Baukus, A. T. Hunter, J. N. Schulman, and J. P. Faurie, J. Appl. Phys. **64**, 283 (1988).
[25] C. L. Cesar, M. N. Islam, R. D. Feldman, R. Spitzer, R. F. Austin, A. E. DiGiovanni, J. Shah, and J. Orenstein, Appl. Phys. Lett. **54**, 745 (1989).
[26] G. L. Hansen, J. L. Schmit, and T. N. Casselman, J. Appl. Phys. **53**, 7099 (1982).